

# The Utility of *R*-Curves for Understanding Fracture Toughness-Strength Relations in Bridging Ceramics

J. J. Kruzic,<sup>\*,†,‡</sup> R. L. Satet,<sup>\*,§,††</sup> M. J. Hoffmann,<sup>\*\*,§</sup> R. M. Cannon,<sup>\*\*,¶,‡‡</sup> R. O. Ritchie<sup>\*,¶,||</sup>

<sup>‡</sup>Materials Science, School of Mechanical, Industrial, and Manufacturing Engineering, Oregon State University, Corvallis, Oregon 97331

<sup>§</sup>Institute for Ceramics in Mechanical Engineering, University of Karlsruhe, D-76131 Karlsruhe, Germany

<sup>¶</sup>Materials Sciences Division, Lawrence Berkeley National Laboratory, Berkeley, California 94720

<sup>||</sup>Department of Materials Science and Engineering, University of California, Berkeley, California 94720

**The mechanical behavior of four rare earth (RE)-Mg-doped Si<sub>3</sub>N<sub>4</sub> ceramics (RE = La, Lu, Y, Yb) with varying grain-boundary adhesion has been examined with emphasis on materials containing La and Lu (which represent the extremes of RE ionic radius). Fracture-resistance curves (*R*-curves) for all ceramics rose very steeply initially, giving them exceptional strength and relative insensitivity to flaw size. The highest strength was seen in the Lu-doped material, which may be explained by its steeper initial *R*-curve; the highest “apparent” toughness (for fracture from millimeter-scale micronotches) was seen in the lowest strength La-doped material, which may be explained by its slowly rising *R*-curve at longer crack lengths. Excellent agreement was found between the predicted strengths from *R*-curves and the actual strengths for failures originating from natural flaws, a result attributed to careful estimation of the early part of the *R*-curve by deducing the intrinsic toughness, *K*<sub>0</sub>, and the fact that this portion of the *R*-curve is relatively insensitive to sample geometry. Finally, it was found that RE elements with relatively large ionic radius (e.g., La) tended to result in lower grain-boundary adhesion. This implies that there is a small window of optimal grain-boundary adhesion which can lead to the fastest rising *R*-curves (for short cracks) and the highest strengths. The importance of this work is that it reinforces the notion that factors which contribute to the early part of the *R*-curve are critical for the design of ceramic microstructures with both high strength and high toughness.**

## I. Introduction

**M**ONOLITHIC ceramics can now be developed with microstructures that promote significant extrinsic toughening<sup>††</sup>; these materials tend to exhibit superior strength and fracture

toughness, properties which result in a wider range of potential commercial applications. One successful approach is to sinter ceramics, such as Si<sub>3</sub>N<sub>4</sub>, SiC, or Al<sub>2</sub>O<sub>3</sub>, with additives that give (i) sufficiently weak grain boundaries and (ii) bimodal grain distributions and/or high aspect ratio self reinforcing grains.<sup>1–8</sup> These structures fail predominantly intergranularly, which leads to extrinsic toughening via crack deflection and crack bridging. Although the basic microstructural features which promote this behavior are well-known, the details of how those features relate to overall strength and toughness are still not well understood, which sometimes leads to unexpected results. For example, consider recent studies where a series of Si<sub>3</sub>N<sub>4</sub> ceramics were sintered with MgO along with various rare-earth oxides (RE<sub>2</sub>O<sub>3</sub>) in order to systematically vary the grain-boundary adhesion while keeping the morphology of the microstructures essentially invariant.<sup>9,10</sup> Using a large RE<sup>3+</sup> cation such as La<sup>3+</sup> gave, as was anticipated, the weakest boundaries, the most observed grain bridging, and the highest toughness as measured by micronotched bend beams; however, the La-doped material unexpectedly exhibited the lowest flexural strength (Fig. 1). Furthermore, the converse was true for the materials doped with the relatively small cation Lu<sup>3+</sup>, which exhibited less bridging and the lowest micronotch toughness, yet the highest strength (Fig. 1). Unpaired Student's *t*-tests (*N* = 5 for toughness, *N* = 30 for strength) show that these differences are statistically significant; indeed, for both properties the La and Lu doped samples are significantly different with *p* < 0.0001. Furthermore, one of the intermediates for the toughness (Yb), and all three for the strength (Yb, Y, Sm), are significantly different than both the La and Lu extremes.

Such results clearly indicate that developing microstructures that simply promote more bridging and a higher apparent (single-value) fracture toughness may not give the best overall mechanical properties, in particular a combination of high strength and toughness. This suggests that a more sophisticated understanding of the interrelations between fracture toughness, strength, and grain-boundary adhesion is needed to optimize ceramic microstructures for structural applications. Accordingly, the purpose of this paper is to present a further examination of these same RE–Mg-bearing silicon nitrides; new results along with recent observations on other bridging ceramics are used to provide a more comprehensive picture of the fracture toughness, strength, and grain-boundary adhesion relationship in grain-bridging ceramics. Additionally, the usefulness of carefully constructed *R*-curves for predicting the behavior of naturally occurring flaws, in terms of the fracture strength, is demonstrated.

## II. Background

Extrinsic toughening via grain-bridging involves intact grains that span across the crack flanks and sustain part of the

C. Landis—contributing editor

Manuscript No. 23975. Received November 14, 2007; approved January 15, 2008.

J. J. K. acknowledges financial support from the National Science Foundation CAREER Award No. 0547394. ROR and RMC acknowledge support from the Director, Office of Science, Office of Basic Energy Science, Division of Materials Sciences and Engineering of the Department of Energy under Contract No. DE-AC02-05CH11231. M. J. H. and R. L. S. thank the DFG Center of excellence (SFB 483) “High Performance Sliding and Friction Systems Based on Advanced Ceramics” for their financial support.

<sup>\*</sup>Member, The American Ceramic Society.

<sup>\*\*</sup>Fellow, The American Ceramic Society.

<sup>†</sup>Author to whom correspondence should be addressed. e-mail: jamie.kruzic@oregonstate.edu

<sup>††</sup>Current Address: Robert Bosch GmbH, D-70049 Stuttgart, Germany.

<sup>‡‡</sup>Deceased.

<sup>||</sup>Unlike intrinsic toughening which involves resistance to damage mechanisms developed ahead of the crack tip, extrinsic toughening is associated with mechanisms of crack-tip shielding which are largely active behind the crack tip. As it involves phenomena active in the crack wake, extrinsic toughening, which can be associated with such mechanisms as crack bridging, constrained microcracking and transformation toughening, will be dependent upon crack size; this will lead to resistance-curve (*R*-curve) toughening behavior.

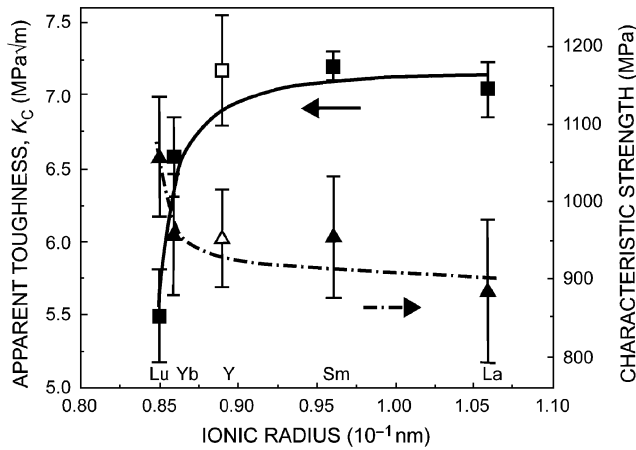


**Fig. 1.** Plot from Satet *et al.*<sup>10</sup> showing the increase in apparent toughness (square symbols), but decrease in strength (triangle symbols), with increasing ionic radius of the RE element. For toughness the mean of five tests is given, and the error bars represent the standard deviation. For strength, Weibull analysis was carried out and the characteristic strength is given, with the error bars representing the 95% confidence intervals.

applied load that would otherwise be experienced at the crack tip, thereby effectively toughening the material by lowering the near-tip stress intensity,  $K_{tip}$ , relative to the applied stress intensity,  $K_{app}$ , thus:

$$K_{tip} = K_{app} - K_{br} \quad (1)$$

where  $K_{br}$  is the bridging stress intensity. Grain bridging occurs as a result of intergranular fracture, and accordingly, the boundaries must be sufficiently weak to provide a preferential crack path. Assuming a pull-out based model in which the maximum pull-out distance of the grain-bridging zone is invariant, a reduction in boundary adhesion, and accordingly the local intrinsic fracture resistance at the boundary, should increase the steady-state bridging, as  $K_{br} \propto 1/K_{tip}$ ,<sup>11–13</sup> by allowing for more high-angle deviations from the mode I crack path that should give a more tortuous path, more bridging, and less transgranular fracture. In consequence, higher toughness might be expected when lowering the boundary adhesion in polycrystals as well. This would be consistent with behavior in brittle matrix composites, where it is well known that lowering the fiber-matrix interface toughness or sliding resistance yields more pull-out and greater net toughening.<sup>14–16</sup> This has sometimes led to an expectation that the fiber/matrix interfaces should be as weak as possible to achieve high toughness for brittle matrix composites. However, even for long fiber composites it has more recently been recognized that if the pull-out length is extremely long it can eventually become detrimental. Thus, there is a trade-off between achieving ever high values of apparent toughness, and the peak strength being reduced by fiber failure which increases in probability as the length of loaded fiber increases.

In monolithic bridging ceramics, overly weak boundaries may similarly degrade strength by essentially flattening the early portion of the *R*-curve. This has been observed in a study on alumina where instead of changing the boundaries themselves, the environment was altered to affect the grain-boundary strength.<sup>17</sup> Experiments performed in a moist (laboratory air) environment showed that the intrinsic boundary toughness,  $K_0$ , was roughly 30% lower than when tested in a dry  $N_2$  environment. Additionally, the *R*-curves rose initially more slowly in moist air, eventually crossing over with the dry *R*-curves after several millimeters of growth. Steep initial slopes are highly desirable for *R*-curves because allowable flaws in ceramics are necessarily small due to the overall low magnitude of the toughness; hence, materials that achieve high toughness at small crack lengths also achieve high strength. Indeed, there are

considerable data in the literature to support the higher strength of alumina in dry relative to moist environments,<sup>13,18–22</sup> although it is only recently that the changing *shape* of the *R*-curve has been shown to be a key contributor to this effect.<sup>17</sup>

Such results imply that there is a small “window” of optimal grain-boundary strength for promoting both high strength and fracture resistance in bridging ceramics. While excessively strong boundaries lead to transgranular cracking with neither bridging nor toughening, it appears that overly weak boundaries are also detrimental due to shallower *R*-curves and lower resultant strengths. The present paper seeks to examine new and previous results on RE–Mg oxide doped silicon nitride ceramics in this context to better understand the interrelations between fracture toughness, strength, and grain-boundary adhesion.

### III. Experimental Procedures

#### (1) Materials

Ceramic bulk samples of the five-component system Si–RE–Mg–O–N (with RE = La, Lu, Y, or Yb) were prepared with a constant composition in equivalent percent so that all compositions contained the same atomic amount of the RE element.<sup>88</sup> Full details on materials preparation may be found in Satet and Hoffmann,<sup>9</sup> but briefly, powders were prepared by attrition milling in isopropanol and the slurries were subsequently dried and the powders sieved. Green bodies were uniaxially pressed and then subsequently cold-isostatically pressed with 400 MPa. Samples of different compositions were sintered at different temperatures and dwell times in order to tailor the microstructures to essentially equivalent grain sizes and morphologies. The samples were sintered in a hot-isostatic-press (HIP) with a two-step sinter-HIP process, where closed porosity is obtained at low  $N_2$  pressures during the first sintering step and full density is achieved during the subsequent HIP step at a maximum nitrogen pressure of 10 MPa. Full density (water immersion method) is defined here for relative densities >99% of theoretical density, which was calculated by the rule of mixtures based on the starting compounds.

Additionally, to further investigate the crack kinking behavior of individual grains, oversaturated RE–Si–Mg oxynitride glasses using RE = La, Lu were prepared such that isolated silicon nitride grains were precipitated in a glass matrix approximating the grain-boundary phase composition in the above ceramics. Full details on the preparation of these samples can be found elsewhere,<sup>10,23</sup> and accordingly are only briefly outlined here. Powder mixtures were prepared by ball milling the proper amount of  $Si_3N_4$ ,  $SiO_2$ , MgO, and  $RE_2O_3$  for 1 h in isopropanol using  $Si_3N_4$  grinding media. The equivalent ratio for the cations was maintained constant at 20RE:60Si:20Mg and the  $Si_3N_4$  content exceeded the solubility of each glass by 2–4 eq%. Depending on the molar mass of the rare-earth (RE), this corresponds to 1.3–1.5 vol% of  $Si_3N_4$  available to precipitate out of the glass. Glass beads were prepared by heating cold-isostatically pressed green bodies for 0.5 h at 1710°C under 2 MPa of  $N_2$  and subsequently shutting off the furnace giving a cooling rate of 25°C/min between 1710° and 1100°C. Subsequently, cyclic annealing was performed at 1600°C to precipitate  $Si_3N_4$  grains and monitor grain growth, while the total annealing time for the samples used in this study was 18 h.

#### (2) Fracture Testing

To determine *R*-curves, i.e., fracture resistance,  $K_R$ , as a function of crack extension,  $\Delta a$ , standard compact-tension, C(T), specimens (width,  $W \approx 19$  mm; thickness,  $B \approx 3.5$  mm) were machined from the fully dense pieces. Each specimen was razor micronotched to achieve small notch root radii,  $\rho \approx 15$   $\mu$ m, by repeatedly sliding a razor blade over the machined notch in the presence of a 1  $\mu$ m diamond slurry. Razor-notched samples were

<sup>88</sup>The term rare-earth (RE) will be used here in a broader acceptance for both lanthanides and the chemically similar Group IIIB additives

then precracked by cycling using servo-hydraulic test machines (25 Hz sine wave, load ratio  $R = P_{\min}/P_{\max} = 0.1$ ) while occasionally raising  $P_{\max}$  until the onset of cracking, as revealed by an increase in compliance (i.e., slope of the back-face strain versus load curve).  $R$ -curve tests were then conducted by loading the precracked specimens in displacement control while episodically unloading by  $\sim 10\%$ – $20\%$  of the peak load to ascertain the crack lengths.<sup>24</sup> Crack lengths were monitored during the occasional partial unloading based on strain gauges mounted on the back face of the specimen along with standard C(T) compliance calibrations.<sup>25</sup> Crack lengths were periodically verified by unloading the specimens and examining them using optical microscopy. Discrepancies in the crack length were corrected by assuming that the error accumulated linearly with crack extension over the portion of the  $R$ -curve just previously measured. Fatigue precracks were grown only to  $\Delta a_f = \sim 20$ – $200$   $\mu\text{m}$  before measuring  $R$ -curves to minimize the initial bridging, where  $\Delta a_f$  is the length of the fatigue-crack extension from the machined notch, i.e.,  $\Delta a_f = a - a_0$ . Here,  $a$  refers to the crack length at any given time, and  $a_0$  refers to the initial notch length. Such initial crack lengths were long enough to not be affected by the presence of the micronotches; indeed, the effect of the notch field is effectively diminished once the crack has extended a distance of at least one root radius,  $\rho$ , away.<sup>26</sup>

### (3) Crack Profiles and $K_0$ Determination

Qualitative observations of crack paths and fracture surfaces were made using a field-emission scanning electron microscope (FESEM). Additionally, to assess the magnitude of the intrinsic toughness,  $K_0$ , crack-opening displacements,  $u(x)$ , were measured quantitatively on samples loaded *in situ* in the FESEM, where  $x$  is the position along the crack wake with origin at the load line. The crack-opening displacement data were used to directly deduce estimates for the intrinsic toughness,  $K_0$ , using a two-term solution for the shape of a bridged crack<sup>27</sup>:

$$u(x) = \frac{K_0}{E'} \int_x^a h(x, a') da' + \frac{A_1}{E'} \int_x^a (aa') h(x, a') da' \quad (2)$$

In Eq. (2),  $E'$  is the plane strain modulus ( $E' = E/(1-\nu^2)$  where  $E$  is Young's modulus and  $\nu$  is Poisson's ratio) and the unknowns  $K_0$  and  $A_1$  may be determined using a least-squares fit to the experimental  $u(x)$  data. In both cases,  $h$  for the C(T) specimen was used, viz<sup>28</sup>:

$$h = \sqrt{\frac{2}{\pi a}} \frac{1}{\sqrt{1-x/a}} \times \left[ 1 + \sum_{(\nu, \mu)} \frac{A_{\nu\mu} (a/W)^\mu}{(1-a/W)^{3/2}} (1-x/a)^{\nu+1} \right] \quad (3)$$

where the coefficients  $A_{\nu\mu}$  are given in Fett and Munz.<sup>28</sup> This method was used for one La and one Lu-doped specimen.

### (4) Crack Kinking Experiments

To directly investigate variations in the adhesion between the silicon nitride grains and the grain-boundary glass phase, a method similar to that developed by Becher *et al.* was used.<sup>29,30</sup> Specifically, Vickers indents were placed with a 1 N load in the oversaturated oxynitride glass samples in the vicinity of various  $\text{Si}_3\text{N}_4$  grains in order to generate cracks that impinged on the  $\text{Si}_3\text{N}_4$  grains (Fig. 2). The angle of incidence,  $\theta$ , was varied and the length of the debond,  $l_{\text{db}}$ , of the interface between the grain and the glass was measured in a SEM. During these experiments, the ratio of the intersecting crack length,  $l_{\text{int}}$ , to the nominal crack length,  $l_0$ , was kept approximately constant,  $l_{\text{int}}/l_0 \sim 0.5$ .

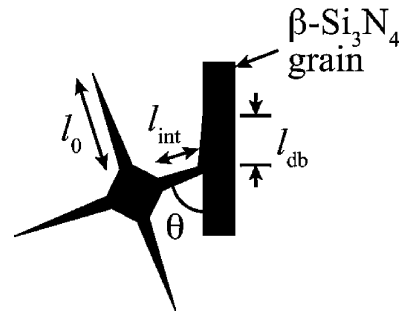


Fig. 2. Schematic of the interfacial adhesion tests using Vickers indents.

### (5) Critical Flaw Size Evaluation

To correlate four-point bending strength data from previous studies<sup>9,10</sup> with the  $R$ -curve data from the present study, careful SEM analysis of the fracture surfaces of the failed bending beams was conducted to assess the radius of the critical flaws that caused fracture. In those studies, 3 mm  $\times$  4 mm  $\times$  50 mm unnotched beams were loaded in four-point bending until failure and the resulting strengths reported on the basis of the maximum flexure stress. In this study, those strength values were revised based on the stress level at the actual flaw location rather than the maximum bending stress to give an effective strength that directly corresponds with the individual flaws.  $R$ -curve data were then used to predict the strength of each  $\text{Si}_3\text{N}_4$  material as a function of initial flaw size using standard techniques based on the stress intensity equation for a penny shaped flaw.<sup>31</sup> The applied stress,  $\sigma_{\text{app}}$ , equals the fracture strength for an initial penny shaped flaw radius of  $a_i$  when the following two conditions are satisfied:

$$K_{\text{app}} = 2\sigma_{\text{app}} \sqrt{\frac{\Delta a + a_i}{\pi}} = K_R \text{ and } \frac{dK_{\text{app}}}{da} = \frac{dK_R}{da} \quad (4)$$

where  $K_R$  is the fracture resistance from the  $R$ -curve. Predictions based on Eq. (4) and the  $R$ -curve data are then compared with the actual strength-flaw size data.

## IV. Results

### (1) $R$ -Curve and $K_0$ Results

$R$ -curve results were limited owing to experimental difficulties. Although three or four specimens were precracked for each composition, specimens with highly asymmetric precracks were excluded from  $R$ -curve testing. As a result, only one or two  $R$ -curves were obtained for each material, as illustrated in Fig. 3. In this figure, part (a) shows the fracture resistance in terms of the absolute stress intensity; it also shows the deduced  $K_0$  values for the La-, Lu-, and Y-doped materials as well as a range of reported  $K_c$  values ( $\sim 2.0$ – $2.2$   $\text{MPa} \cdot \text{m}^{1/2}$ ) for transgranular fracture in  $\text{Si}_3\text{N}_4$  where the  $R$ -curve is flat.<sup>32,33</sup> The  $K_0$  value for the Y-doped sample was taken from another study where micro Raman spectroscopy was used to measure the bridging stresses.<sup>34</sup> In all cases, the deduced  $K_0$  values for the present materials fall below the  $K_0$  values for transgranular fracture, as is expected due to the weaker intergranular crack path.

Figure 3(b) shows the same  $R$ -curves normalized to the nominal "peak" toughness for each material, which is useful for making a more clear comparison of the  $R$ -curve shape for each material. A dramatic difference in  $R$ -curve shape is seen when comparing the Lu and La-doped  $R$ -curves. The  $R$ -curve for the La-doped sample rises initially more slowly at short crack lengths, and continues to rise over 2 mm of crack extension until the test was concluded. Conversely, the Lu-doped material reached its peak toughness much more quickly, followed by a gradual loss in fracture resistance with further extension. Although the data are incomplete at the shortest crack lengths, the Y-doped sample also exhibits a similar decline in fracture

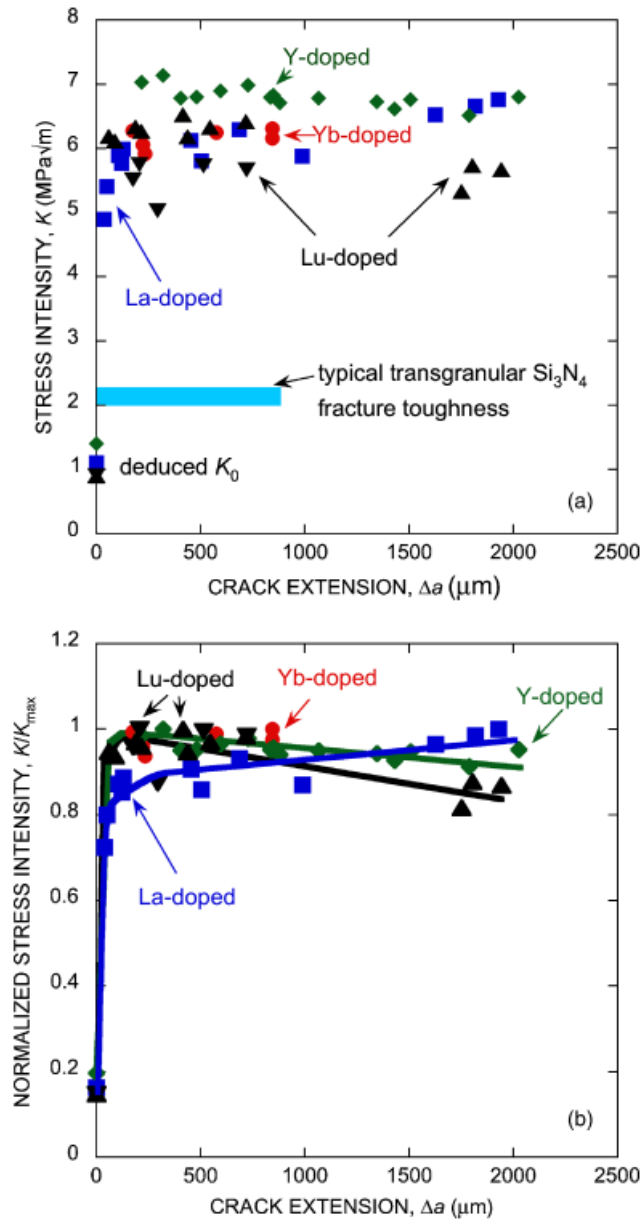


**Fig. 3.** *R*-curves measured for various RE<sub>2</sub>O<sub>3</sub>-doped Si<sub>3</sub>N<sub>4</sub> ceramics using fatigue precracked C(T) specimens. In (a), the *R*-curves are given in terms of the actual stress intensity, while in (b), the *R*-curves were normalized to the peak toughness to clearly show the change in shape with sintering additive. Values of *K*<sub>0</sub> were deduced for two samples (La and Lu doped) from measured crack-opening profiles in *R*-curve samples, while *K*<sub>0</sub> for Y-doped material was taken from Krzic *et al.*<sup>34</sup> Also shown are typical data for a Y<sub>2</sub>O<sub>3</sub> doped Si<sub>3</sub>N<sub>4</sub> that exhibits transgranular fracture.

resistance after an initial peak toughness value is achieved. Data for the Yb-doped material are too limited to make any detailed comparisons.

## (2) Crack Kinking Results

Qualitative observations of crack paths in previous studies have suggested that the tendency for the crack to kink increases with increasing ionic radius of the RE<sup>3+</sup> cation.<sup>9,10</sup> Figure 4 shows quantitative data comparing the behavior of the La-doped material, with the largest ionic radius, to the Lu-doped material, with the lowest ionic radius. In Fig. 4, it is clearly seen that the critical angle of incidence,  $\theta$ , for glass-Si<sub>3</sub>N<sub>4</sub> debonding is much lower in the Lu-doped material compared with the La-doped material, indicating greater adhesion between the glass and Si<sub>3</sub>N<sub>4</sub> grains. This implies greater crack kinking ability for the

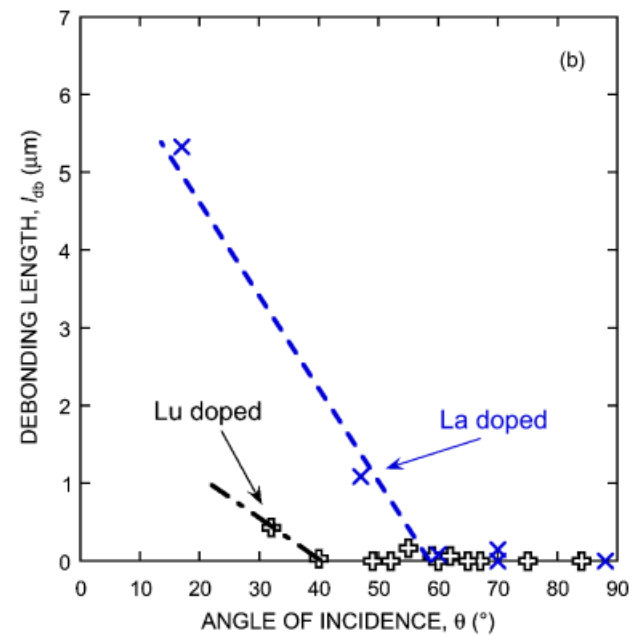
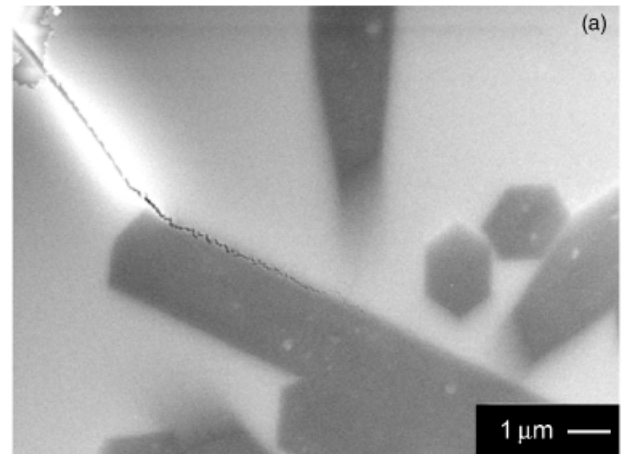


**Fig. 4.** (a) A representative micrograph of a crack impinging upon a Si<sub>3</sub>N<sub>4</sub> grain and causing debonding. (b) The debonding length, *l*<sub>db</sub>, is plotted as a function of the incident angle,  $\theta$ . The critical angle of incidence is clearly lower for the Lu doped sample, indicating stronger adhesion between the glass and the Si<sub>3</sub>N<sub>4</sub> grain.

La-doped Si<sub>3</sub>N<sub>4</sub> bulk ceramic samples, as has been qualitatively observed previously.

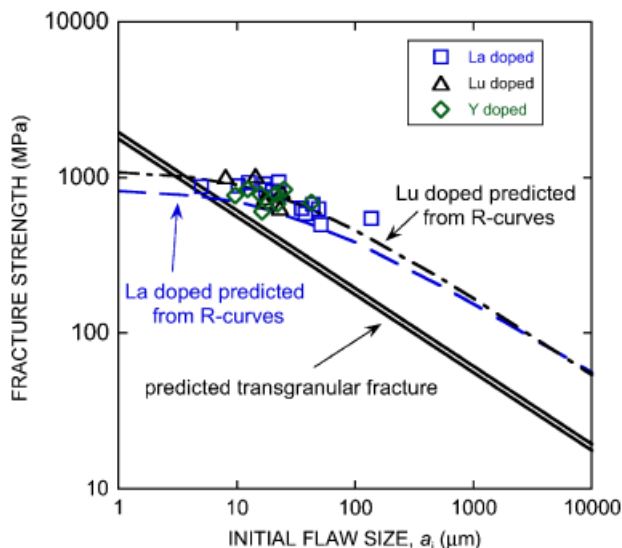
## (3) Strength-Flaw Size Results

Figure 5 shows a plot of effective four-point bending strength as a function of the initial flaw size (radius) determined from the fractographic examinations. In general, flaws in all the samples were similar in appearance and were either voids or inclusions, one example of each is shown in Fig. 6. Also shown is the expected trend for untoughened Si<sub>3</sub>N<sub>4</sub> with transgranular fracture (flat *R*-curve) assuming a simple penny-shaped crack (flaw) using the equation:

$$\sigma_{\text{frac}} = \frac{K_{Ic}}{2} \sqrt{\frac{\pi}{a}} \quad (5)$$

where  $\sigma_{\text{frac}}$  is the fracture strength, *a* is the flaw radius, and *K*<sub>Ic</sub> is the fracture toughness (~2.0–2.2 MPa · m<sup>1/2</sup>). By comparing the data to Eq. (5), it can be seen that the strength of these RE-Mg-doped Si<sub>3</sub>N<sub>4</sub> ceramics are much less sensitive to flaw size than their untoughened counterparts, as is expected.





**Fig. 5.** The measured effective fracture strengths of four-point bending beams from Satet *et al.*,<sup>9,10</sup> here plotted as a function of the initial flaw size determined from fractographic examination. Also shown is the expected trend for untoughened  $\text{Si}_3\text{N}_4$  with transgranular fracture (flat  $R$ -curve) assuming a penny-shaped flaw. It is apparent the strength of these RE-Mg-doped  $\text{Si}_3\text{N}_4$  ceramics are much less sensitive to flaw size than their untoughened counterparts. Finally, predictions of the strength flaw size relations made from the  $R$ -curves are shown for the Lu- and La-doped materials. Note the good agreement with experimental data and the predicted crossover at large flaw sizes.

Also shown in Fig. 5 are the strength predictions made using the  $R$ -curve data from Fig. 3 and Eq. (4). Figure 7 shows a close up view of the early part of the  $R$ -curve, including the estimated behavior between  $K_0$  and the first data point and a graphical example of how the fracture strengths were deduced. For a given initial flaw size, Eq. (4) is satisfied for the stress that causes the  $K_{\text{app}}$  curve (dashed line) to just become tangent to the  $K_R$  curve (solid line). In Fig. 7, an example is shown for an initial flaw size of 40  $\mu\text{m}$ .

Several features about the strength predictions are worth noting. First, there is generally good agreement between the experimental strength data and the predicted curves. Second, the strength of the Lu-doped material is predicted to be higher over the range of flaw sizes relevant for naturally occurring flaws (i.e.,  $\leq 100 \mu\text{m}$ ), which is in agreement with the effective strength results. While one might argue slightly different early  $R$ -curves could be drawn, this does not change the good overall matching with the data. Finally, there is a predicted crossover in the strength for millimeter scale flaws, which is in general agreement with the toughness results obtained in Satet *et al.*<sup>9,10</sup> that used 1–1.2 mm long razor micronotches to assess the fracture toughness.

## V. Discussion

### (1) $R$ -Curves and Strength Predictions

First, we note that although it is not usually considered as such, the  $R$ -curves for extrinsically toughened ceramics should necessarily initiate at a stress-intensity level at or below that to crack a grain (i.e., a single crystal),  $K_{\text{sx}}$ , and generally closer to the level for cracking a grain-boundary facet,  $K_{\text{gb}}$ , because these ceramics largely fracture intergranularly. After initiation, the  $R$ -curve should then rise as extrinsic toughening develops until possibly attaining a steady-state (plateau) value if the specimen dimensions are large relative to the bridging zone size. A recent review by Munz<sup>35</sup> brings attention to the problem that most published  $R$ -curves for macroscopic cracks do not agree with those measured for natural flaws. However, invariably all the macrocrack  $R$ -curves discussed in that paper

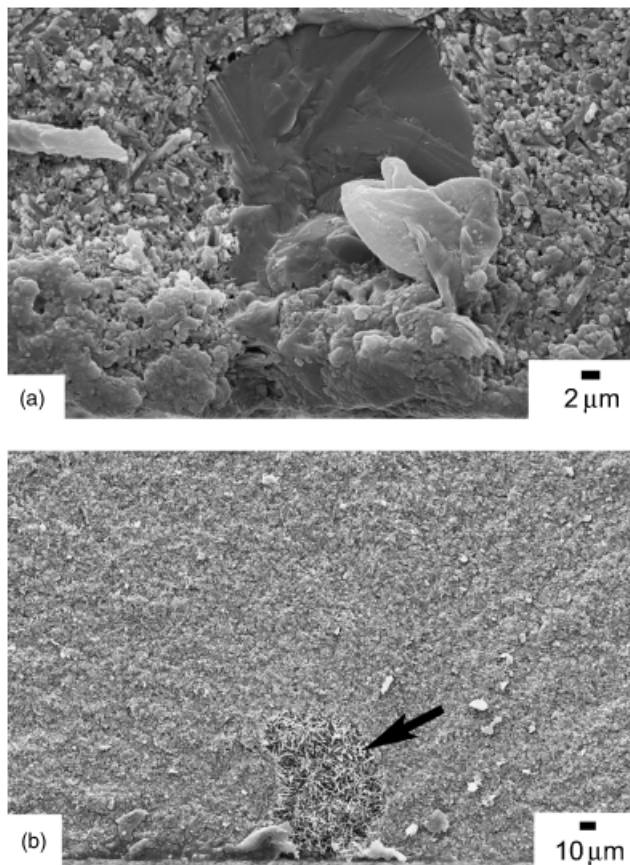


**Fig. 6.** Typical flaws that caused failure in the four-point bend strength samples and that were measured to produce Fig. 5: (a) shows an inclusion in a Lu-doped sample, while (b) shows a void marked by the arrow in a La-doped samples. Both types of flaws were commonly found in all the samples.

begin at stress-intensity values *well above the single crystal toughness*. There are several reasons why this issue persists throughout the  $R$ -curve literature.

1. *Pre-existing extrinsic toughening for long precracks.* Often  $R$ -curves using macroscopic cracks are measured from either fatigue or quasistatically induced precracks that may be several millimeters in length.<sup>36–40</sup> However, even when the sample is fatigue cycled near the fatigue threshold in order to degrade the toughening, significant toughening can still be associated with the precrack. While this fact is evident from the unrealistically high “initiation” values on  $R$ -curves from fatigue precracks,<sup>36–40</sup> more recently this has been demonstrated using combined fatigue and crack-opening profile experiments for a bridging alumina.<sup>34,41</sup>

2. *Overdriving cracks grown from notches.* A second approach to measuring  $R$ -curves involves growing cracks directly from starter notches.<sup>42–44</sup> In this case, the issue of preexisting extrinsic toughening is eliminated; however, due to the lower stress concentration around a blunt notch relative to a sharp crack, the initiation point of the  $R$ -curve is invariably overestimated. This is because a crack coming from a notch is overdriven, and there is invariably an unstable jump in crack length.<sup>45</sup> Then, until the crack extends more than  $\sim 1$  notch root radius,  $\rho$ , the stress intensity at the crack tip is further affected by the notch.<sup>46</sup> This situation has recently been examined in detail by Fett and Munz.<sup>45</sup>

3.  *$R$ -curves initially rise very quickly.* In the present and other recent studies,<sup>17,41</sup> care has been taken to measure the  $R$ -curve from the shortest precracks possible, using sharp razor micronotches, and ensuring that  $a_{\text{precrack}} > \rho$  in an attempt to attain the best attributes of both methods listed above. However, as can be seen in Fig. 3 and Kruzic *et al.*,<sup>17,41</sup> the  $R$ -curves generally rise so steeply that the first data points collected are

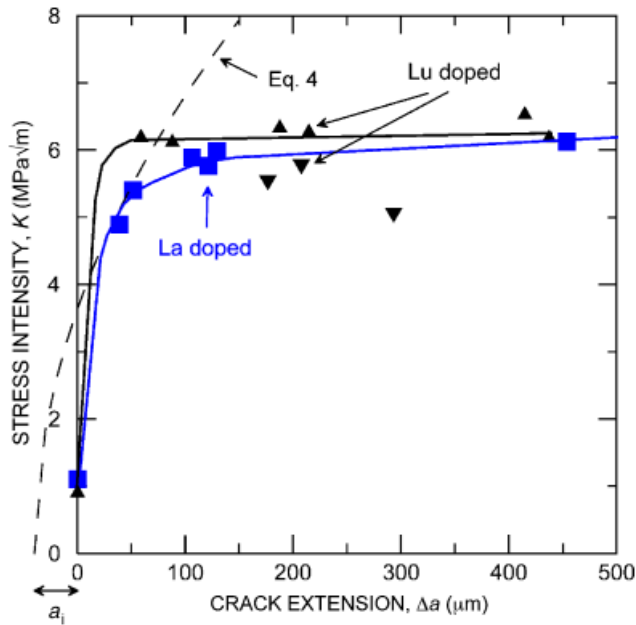


**Fig. 7.** Close-up view of the early  $R$ -curves for the Lu and La-doped silicon nitrides illustrating how the  $R$ -curves determine the strength versus flaw size predictions in Fig. 5. Note, at small initial flaw sizes,  $a_i$ , the early part of the  $R$ -curve is the most important for determining the strength. In this example, Eq. (4) (dashed line) is plotted for  $a_i = 40 \mu\text{m}$  and an applied stress of 510 MPa which is the predicted fracture strength for the La-doped  $\text{Si}_3\text{N}_4$  at that flaw size.

well above any reasonable value for the intrinsic toughness. Insight into the cause of this steep initial rise has recently been obtained through cohesive-zone modeling,<sup>47</sup> and will be discussed further in Section V(3).

Additionally, this situation is clouded by two factors, namely: (i) for a very *small* crack having all areal dimensions of the order of the grain size, the effects of local residual stresses, e.g., from thermal expansion mismatch, may influence the effective toughness, even lowering it below that for the boundary facet for a critical flaw<sup>11–13</sup>; or (ii) for a very *short* crack, which in the hypothetical limit is a ribbon of through-thickness crack but with  $a$  being less than a grain facet long, the residual stress effects tend to cancel, but the inevitable kinks and twists raise the initiation toughness above the average for the actual boundary facets.<sup>48</sup> Regardless, *the early part of the  $R$ -curve is most important for reliability and strength*, although it is rarely measured accurately, if at all, in studies using macroscopic cracks.

Recently, a hybrid approach has been developed whereby the  $R$ -curve is measured using traditional macrocrack specimens, but beginning with micro-scale short precracks emanating from razor micronotches. These  $R$ -curve measurements are then supplemented by separate experiments to assess the intrinsic toughness either by measuring the crack-opening displacements or by using micro Raman spectroscopy, and the early part of the  $R$ -curve in drawn back to that point.<sup>17,34,41</sup> While those authors have conjectured that such an approach should allow reasonably accurate predictions of short and/or small cracks, the results in Fig. 5 represent the first verification that this method can reasonably predict the behavior of naturally occurring flaws.

The predicted curve for the Lu-doped material demonstrates remarkable agreement with the experimental data, while the curve for the La-doped material appears slightly underestimated. Furthermore, the predicted flaw size where the strengths should cross-over is somewhat overestimated. The notches used to obtain the fracture toughness data in Fig. 1 were on the order of 1–1.2 mm in length, so the true crossover size should be on the order of 100's of micrometers rather than several millimeters

as is predicted in Fig. 5. Both of these inconsistencies are likely due, at least in part, to a slight underestimation in the steepness of the early  $R$ -curve for the La-doped material. Indeed, a slightly steeper  $R$ -curve would shift the La-doped predictions up, improving the agreement for both the strength data and the cross-over flaw size. Based on the  $R$ -curve data in Fig. 7, arbitrarily drawing a steeper  $R$ -curve would be inappropriate; however, with improvements in techniques to obtain the early part of  $R$ -curves it is expected that the agreement with the experimental data will also improve. Methods based on measuring the bridging stress distribution and deducing the early  $R$ -curve appear to be especially useful here when coupled with carefully measured  $R$ -curve data.

Finally, the question remains why, when previous studies have shown unequivocally that sample geometry can affect  $R$ -curve shapes,<sup>48,49</sup> do the  $R$ -curves from C(T) specimens provide a good estimate of the behavior of natural flaws in bend beams. To answer this question, it must be recognized that there is a distinct difference between the  $\text{Si}_3\text{N}_4$  ceramics in the present study and the coarse-grained aluminas in those studies. Coarse-grained aluminas have slowly rising  $R$ -curves and bridging zones that extend generally extend  $> 10 \text{ mm}$  in length, often too long to ever reach a steady-state plateau toughness with regular-sized specimens.<sup>41,49–51</sup> Clearly a large-scale bridging condition exists for those experiments; indeed, the bridging-zone size is often similar to the specimen dimensions. It is generally thought that the bridging-zone length is dictated by a critical crack opening, beyond which all bridges must fail. Thus, since the crack-opening profile for cracks on the millimeter scale in typical samples will be dictated by the overall sample geometry, it is clear that the bridging-zone length and the shape of the  $R$ -curve will similarly be geometry dependent.

In the case of the present silicon nitrides, based on the fast rising  $R$ -curves (Fig. 3) and studies on the fatigue crack bridging zone in the Y-doped material,<sup>34</sup> the expected bridging-zone length is roughly 1–2 orders of magnitude smaller. A condition of small-scale bridging thus exists. Accordingly, the crack-opening profile in the bridging zone will be dictated mostly by the near-tip crack-opening behavior, such as is described the well-known Irwin solution:

$$u(x) = \frac{K_{\text{tip}}}{E'} \sqrt{\frac{8(a-x)}{\pi}} \quad (6)$$

after being corrected for the influence bridging stresses. The notation used in Eq. (6) is identical to that used in Section III(3), and such near-tip crack-opening behavior is insensitive to overall sample geometry because the higher-order terms associated with specimen dimensions become negligible near the crack tip. Accordingly, the  $R$ -curves for the present  $\text{Si}_3\text{N}_4$  ceramics are largely geometry-insensitive for the samples used due to the fact that small-scale bridging conditions prevailed. A possible exception to this is the La-doped material, which shows a slow rise in the  $R$ -curve over at least 2 mm. In that case, the predictions at large flaw sizes may be affected by specimen geometry; indeed, this is another possible reason why the cross-over flaw size was overestimated in Fig. 5. However, it is expected that the early part of the La-doped  $\text{Si}_3\text{N}_4$   $R$ -curve that determines the strength for *natural flaws* would be unaffected by geometry.

Finally, while it is possible that similar correlations between strength and  $R$ -curve behavior will not work as well in coarse-grain aluminas for the above reasons, this is not necessarily the case. Because strength predictions for natural flaws only require the early part of the  $R$ -curve, and the early part of the  $R$ -curve should be largely geometry-independent according to Eq. (6), it is quite possible that good agreement will exist between strength predictions from carefully constructed  $R$ -curves using C(T) specimens and actual measured fracture strengths from samples with natural flaws. Of course, the same would not be expected for large flaws, but they are of significantly less interest compared with natural flaws. In the large flaw case, it should be expected

<sup>48</sup>The terminology used here is that *short* cracks are small only with respect to length, whereas *small* cracks are small with respect to width and length.

that different strategies would become necessary. For example, one approach would be to convert the  $R$ -curve to represent the appropriate sample geometry by deducing or measuring the bridging stress function.<sup>48</sup>

### (2) Intrinsic Effects: Estimation of $K_0$

In this study,  $K_0$  estimates were found to be similar for both the La-doped ( $1.0 \text{ MPa} \cdot \text{m}^{1/2}$ ) and Lu-doped ( $0.9 \text{ MPa} \cdot \text{m}^{1/2}$ ) specimens, and somewhat lower than the value of  $1.4 \text{ MPa} \cdot \text{m}^{1/2}$  obtained in another study for the Y-doped material using Raman spectroscopy methods.<sup>34</sup> All the  $K_0$  values for these RE–Mg-doped  $\text{Si}_3\text{N}_4$  ceramics were lower than for a commercial Y–Al-doped  $\text{Si}_3\text{N}_4$ , where a value of  $1.7 \text{ MPa} \cdot \text{m}^{1/2}$  was found using similar crack-opening profile methods.<sup>52</sup> Clearly, some variation in  $K_0$  should be expected between different  $\text{Si}_3\text{N}_4$  ceramics; however, based on Fig. 4 and previous crack-path observations, it is apparent that  $K_0$  should be lower in the La-doped materials relative to the Lu-doped material. It is important to point out though that in all the above cases, the  $K_0$  values are well below the grain toughness, estimated to be  $K_{\text{sx}} \approx 2.0\text{--}2.2 \text{ MPa} \cdot \text{m}^{1/2}$  from  $\text{Si}_3\text{N}_4$  ceramics that failed transgranularly,<sup>32,33</sup> and thus likely represent something closer to the toughness of the glass phase at the grain boundaries,  $K_{\text{gb}}$ . Indeed, the values obtained in the present study are similar to what has been reported for a Y–Si–Al oxynitride glass,  $\sim 1 \text{ MPa} \cdot \text{m}^{1/2}$ ,<sup>53</sup> which is not unreasonable considering the similar compositions of the grain-boundary phases in the present study. Finally, another study using the Raman spectroscopy based techniques found  $K_0 = 2.7 \text{ MPa} \cdot \text{m}^{1/2}$  for a different Y–Al-doped  $\text{Si}_3\text{N}_4$ , which is a significant overestimate considering that  $K_{\text{sx}} \approx 2.0\text{--}2.2 \text{ MPa} \cdot \text{m}^{1/2}$  and predominantly intergranular fracture was observed.<sup>54</sup>

Based on a two-dimensional model,<sup>55</sup> if the ratio  $K_{\text{gb}}/K_{\text{sx}} \leq 0.5$ , then kinking occurs readily allowing a crack to deflect onto any intersected grain boundary. In that case, the fracture should be entirely intergranular, which is not quite seen here, possibly owing to the simplicity of a two-dimensional representation or to  $K_{\text{gb}}/K_{\text{sx}}$  not being quite so low. Thus, while the  $K_0$  values deduced in this study are likely underestimates, they are not unreasonable and fall at the low end of the expected range.

### (3) Extrinsic Effects: Bridging-Zone Development

Increases in grain-boundary adhesion derived using different additives have been found to yield initially steeper  $R$ -curves in these RE+Mg bearing  $\text{Si}_3\text{N}_4$  ceramics (Fig. 3). Such results are similar to what has been observed in alumina where the grain-boundary strength was altered by changing the environment (moist versus dry) rather than the sintering additives.<sup>17</sup> In that study, it was concluded based on significantly reduced hysteresis in the compliance measurements that the stronger grain boundaries (i.e., dry environment) induced a shift in the predominant bridging mechanism from frictional to uncracked-ligament bridging. Uncracked-ligament bridges are usually seen as regions of intact material, often several grain diameters in size, between noncoplanar crack segments in the wake of a crack tip which form as a result of either nonuniform advance of the crack front (leading to segments subsequently sweeping under and over one another), or nucleation of microcracking ahead of the main crack tip. Measurements of bridging stresses using X-ray fluorescence, Raman spectroscopy, and crack-opening profile techniques on alumina and  $\text{Si}_3\text{N}_4$  have shown a large abrupt drop in bridging stress beyond the regions containing uncracked-ligament bridges, suggesting that these bridges sustain markedly higher stresses than do frictional bridges further behind in the trailing crack wake.<sup>41,54,56–58</sup>

Work on silicon carbide has also shown that changes in the interface chemistry and structure can cause a noticeable shift to more uncracked-ligament versus frictional bridging.<sup>40</sup> In those SiC ceramics, both the nominal fracture resistance and the fatigue threshold were improved with more elastic bridging. Uncracked ligaments were argued to better resist fatigue loading

because frictional wear is less effective for bridge degradation,<sup>40</sup> but concomitant microstructure changes (grain size, aspect ratio) in that SiC study made isolation of the various effects of interface chemistry/structure intractable. However, both the present study, which used nominally the same microstructure for all the materials, and the work of Kruzic et al.<sup>17</sup> on alumina in moist and dry environments, where the microstructure and chemistry remained definitively unchanged, observed similar trends. Thus, based on the collective results on  $\text{Si}_3\text{N}_4$ ,  $\text{Al}_2\text{O}_3$ ,<sup>17</sup> and SiC,<sup>40</sup> it is becoming increasingly clear that shifts to more elastic bridging and the associated steeper  $R$ -curves are likely related to stronger boundaries, and this trend appears to be ubiquitous among bridging ceramics.

Although uncracked-ligament bridges are known to operate nearer to the crack tip than do frictional ones,<sup>41,54,57–60</sup> it has generally been unclear why such bridges should be so strong or cause such a rapid rise in fracture resistance at very small crack lengths. Recent two-dimensional cohesive-zone modeling studies have provided some insight by demonstrating that for a crack intersecting a single grain, significant toughening above that for simple crack kinking is generated during the bridge formation process, even before the crack has propagated far enough for a bridge to form.<sup>47</sup> In that study, depending on the orientation and aspect ratio of the grain, either complete debonding occurs, creating a frictional bridge, or a new crack nucleates ahead, creating an uncracked bridge. While the specific role of boundary strength was not examined in that study, it would seem to follow that stronger boundaries could make the scenario where total debonding occurs less likely, and/or delay the failure of uncracked bridges that do form; this would explain the higher concentration of uncracked bridges observed by Kruzic et al.<sup>17</sup> for alumina.

Evidently, while sufficiently weak boundaries are essential for toughening via bridging in ceramics, it appears that the optimal “window” for boundary strength is small. Indeed, if boundaries are weaker than optimal, the  $R$ -curves rise less steeply, strength is lower, and fatigue is a larger problem due to the higher proportion of frictional bridging. Of course, it is also obvious that too much boundary strength leads to transgranular fracture and no extrinsic toughening, as is well illustrated for specific SiC- or  $\text{Si}_3\text{N}_4$ -based materials.<sup>32,37,61</sup>

## VI. Conclusions

Based on a study of the fracture, strength, and grain-boundary adhesion properties of RE–Mg-doped silicon nitride ceramics, the following conclusions can be made.

1. The  $R$ -curves for all the RE–Mg-doped  $\text{Si}_3\text{N}_4$  ceramics rise initially very steeply at short crack lengths relative to other bridging ceramics ( $\text{Al}_2\text{O}_3$ , SiC) giving them their exceptional strength and relative insensitivity to flaw size.
2. When comparing the extremes of grain-boundary adhesion (Lu and La), the high strength of the Lu-doped material may be explained by the steeper initial  $R$ -curve. Furthermore, the seemingly contradictory higher “apparent” toughness for millimeter-scale micronotches may be explained by the slowly rising  $R$ -curve for the La-doped material at longer crack lengths. Thus, single value toughness assessments can be misleading for understanding the strength of bridging ceramics.
3. There is remarkable agreement between the predicted strengths from  $R$ -curves measured on C(T) specimens and the actual strengths plotted as a function of initial natural flaw size. This good agreement is attributed to careful estimation of the early part of the  $R$ -curve by deducing  $K_0$  and the fact that the early part of the  $R$ -curve should be largely insensitive to sample geometry.
4. There is a systematic effect of the particular RE element on the grain-boundary adhesion, which is related to the trends in strength and toughness. It has been found that those RE elements with large ionic radius tend to give weaker grain-boundary adhesion. Based on present and previous results, there is a “window” of optimal grain-boundary adhesion which gives the fastest rising  $R$ -curves for short cracks and the highest strengths.

If grain boundaries are too strong, transgranular fracture occurs and low toughness and strength result. Conversely, if they are too weak then the  $R$ -curves rise less slowly, although likely achieving higher plateau values eventually.

5. The early part of the  $R$ -curve is the most important as it governs both the strength and toughness of ceramics at realistically small flaw sizes. Factors contributing to this region are critical for designing high strength, damage-tolerant ceramics. Because this is a very difficult regime to study experimentally, it is apparent that much can be learned from further modeling of such behavior.

### Acknowledgments

This paper is dedicated to the memory of one of the authors, Dr. Rowland Cannon, who died suddenly and unexpectedly on April 21, 2006.

### References

- <sup>1</sup>F. F. Lange, "Relation Between Strength, Fracture Energy, and Microstructure of Hot-Pressed  $\text{Si}_3\text{N}_4$ ," *J. Am. Ceram. Soc.*, **56** [10] 518–22 (1974).
- <sup>2</sup>G. Himsolt, H. Knoch, H. Huebner, and F. W. Kleinlein, "Mechanical Properties of Hot-Pressed Silicon Nitride with Different Grain Structures," *Am. Ceram. Soc.*, **62** [1–2] 29–32 (1979).
- <sup>3</sup>P. L. Swanson, C. J. Fairbanks, B. R. Lawn, Y.-W. Mai, and B. J. Hockey, "Crack-Interface Grain Bridging as a Fracture Resistance Mechanism in Ceramics: I, Experimental Study on Alumina," *J. Am. Ceram. Soc.*, **70** [4] 279–89 (1987).
- <sup>4</sup>Y.-W. Mai and B. R. Lawn, "Crack-Interface Grain Bridging as a Fracture Resistance Mechanism in Ceramics: II, Theoretical Fracture Mechanics Model," *J. Am. Ceram. Soc.*, **70** [4] 289–94 (1987).
- <sup>5</sup>N. P. Padture, "In situ-Toughened Silicon Carbide," *J. Am. Ceram. Soc.*, **77** [2] 519–23 (1994).
- <sup>6</sup>N. P. Padture and B. R. Lawn, "Toughness Properties of a Silicon Carbide with an In Situ Induced Heterogeneous Microstructure," *J. Am. Ceram. Soc.*, **77** [10] 2518–22 (1994).
- <sup>7</sup>J. J. Cao, W. J. MoberlyChan, L. C. De Jonghe, C. J. Gilbert, and R. O. Ritchie, "In situ Toughened Silicon Carbide with Al–B–C Additions," *J. Am. Ceram. Soc.*, **79** [2] 461–9 (1996).
- <sup>8</sup>P. F. Becher, E. Y. Sun, K. P. Plucknett, K. B. Alexander, C.-H. Hsueh, H.-T. Lin, S. B. Waters, C. G. Westmoreland, E.-S. Kang, K. Hirao, and M. E. Brito, "Microstructural Design of Silicon Nitride with Improved Fracture Toughness: I, Effects of Grain Size and Shape," *J. Am. Ceram. Soc.*, **81** [11] 2821–30 (1998).
- <sup>9</sup>R. L. Satet and M. J. Hoffmann, "Influence of the Rare-Earth Element on the Mechanical Properties of RE–Mg Bearing Silicon Nitride," *J. Am. Ceram. Soc.*, **88** [9] 2485–90 (2005).
- <sup>10</sup>R. L. Satet, M. J. Hoffmann, and R. M. Cannon, "Experimental Evidence of the Impact of Rare-Earth Elements on Particle Growth and Mechanical Behaviour of Silicon Nitride," *Mater. Sci. Eng. A*, **422** [1–2] 66–76 (2006).
- <sup>11</sup>P. Chantikul, S. J. Bannison, and B. R. Lawn, "Role of Grain Size in the Strength and  $R$ -Curve Properties of Alumina," *J. Am. Ceram. Soc.*, **73** [8] 2419–27 (1990).
- <sup>12</sup>S. J. Bannison and B. R. Lawn, "Role of Interfacial Grain-Bridging Sliding Friction in the Crack-Resistance and Strength Properties of Nontransforming Ceramics," *Acta Metall.*, **37** [10] 2659–71 (1989).
- <sup>13</sup>S. Lathabai and B. R. Lawn, "Fatigue Limits in Noncyclic Loading of Ceramics with Crack-Resistance Curves," *J. Mater. Sci.*, **24** [12] 4298–306 (1989).
- <sup>14</sup>M. D. Thouless, O. Sbaizer, L. S. Sigl, and A. G. Evans, "Effect of Interface Mechanical Properties on Pullout in a SiC-Fiber-Reinforced Lithium Aluminum Silicate Glass-Ceramic," *J. Am. Ceram. Soc.*, **72** [4] 525–32 (1989).
- <sup>15</sup>P. F. Becher, C. H. Hsueh, K. B. Alexander, and E. Y. Sun, "Influence of Reinforcement Contact and Diameter on the  $R$ -Curve Response in SiC-Whisker-Reinforced Alumina," *J. Am. Ceram. Soc.*, **79** [2] 298–304 (1996).
- <sup>16</sup>A. G. Evans, "High Toughness Ceramics," *Mater. Sci. Eng.*, **A105/106**, 65–75 (1988).
- <sup>17</sup>J. J. Kruzic, R. M. Cannon, and R. O. Ritchie, "Effects of Moisture on Grain-Boundary Strength, Fracture and Fatigue Properties of Alumina," *J. Am. Ceram. Soc.*, **88** [8] 2236–45 (2005).
- <sup>18</sup>G. K. Bansal, W. H. Duckworth, and D. E. Niesz, "Strength-Size Relations in Ceramic Materials: Investigation of an Alumina Ceramic," *J. Am. Ceram. Soc.*, **59** [11–12] 472–8 (1976).
- <sup>19</sup>S.-J. Cho, K.-J. Yoon, J.-J. Kim, and K.-H. Kim, "Influence of Humidity on the Flexural Strength of Alumina," *J. Eur. Ceram. Soc.*, **20** [6] 761–4 (2000).
- <sup>20</sup>S.-J. Cho, K.-J. Yoon, Y.-C. Lee, and M.-C. Chu, "Effects of Environmental Temperature and Humidity on the Flexural Strength of Alumina and Measurement of Environment-Insensitive Inherent Strength," *Mater. Lett.*, **57** [18] 2751–4 (2003).
- <sup>21</sup>C. C. McMahon, "Relative Humidity and Modulus of Rupture," *Am. Ceram. Soc. Bull.*, **58** [9] 873 (1979).
- <sup>22</sup>A. G. Evans, "A Method for Evaluating the Time-Dependent Failure Characteristics of Brittle Materials and its Application to Polycrystalline Alumina," *J. Mater. Sci.*, **7**, 1137–46 (1972).
- <sup>23</sup>R. L. Satet and M. J. Hoffmann, "Grain Growth Anisotropy of  $\beta$ -Silicon Nitride in Rare-Earth Doped Oxynitride Glasses," *J. Eur. Ceram. Soc.*, **24**, 3437–45 (2004).
- <sup>24</sup>ASTM *ASTM E561-98*, in *Annual Book of ASTM Standards. Vol. 03.01, Metals- Mechanical Testing; Elevated and Low-temperature Tests; Metallography*, pp. 534–46. ASTM, West Conshohocken, Pennsylvania, USA, 2002.
- <sup>25</sup>D. C. Maxwell *Strain based compliance method for determining crack length for a C(T) specimen*. 1987, Air Force Wright Aeronautical Laboratories.
- <sup>26</sup>A. N. Palazotto and J. G. Mercer, "Crack Considerations in a Notched Compact Tension Specimen," *Eng. Fract. Mech.*, **37** [3] 473–92 (1990).
- <sup>27</sup>A. B. K. Njiwa, T. Fett, D. C. Lupascu, and J. Rödel, "Crack-Tip Toughness of a Soft Lead Zirconate Titanate," *J. Am. Ceram. Soc.*, **86** [11] 1973–5 (2003).
- <sup>28</sup>T. Fett and D. Munz, *Stress Intensity Factors and Weight Functions*. Computational Mechanics Publications, Southampton, UK, 1997.
- <sup>29</sup>P. F. Becher, E. Y. Sun, C. H. Hsueh, K. B. Alexander, S. L. Hwang, S. B. Waters, and C. G. Westmoreland, "Debonding of Interfaces Between Beta-Silicon Nitride Whiskers and Si–Al–Y Oxynitride Glasses," *Acta Mater.*, **44** [10] 3881–93 (1996).
- <sup>30</sup>E. Y. Sun, P. F. Becher, C.-H. Hsueh, G. S. Painter, S. B. Waters, S.-L. Hwang, and M. J. Hoffmann, "Debonding Behavior Between  $\beta$ - $\text{Si}_3\text{N}_4$  Whiskers and Oxynitride Glasses with or without an Epitaxial  $\beta$ -SiAlON Interfacial Layer," *Acta Mater.*, **47** [9] 2777–85 (1999).
- <sup>31</sup>T. L. Anderson, *Fracture Mechanics: Fundamentals and Applications*, 3rd edition, Taylor and Francis Group, Boca Raton, FL, 2005.
- <sup>32</sup>M. J. Hoffmann, A. Geyer, and R. Oberacker, "Potential of the Sinter-HIP-Technique for the Development of High-Temperature Resistance  $\text{Si}_3\text{N}_4$ -Ceramics," *J. Eur. Ceram. Soc.*, **19** [13–14] 2359–66 (1999).
- <sup>33</sup>A. Ziegler, J. M. McNaney, M. J. Hoffmann, and R. O. Ritchie, "On the Effect of Local Grain-Boundary Chemistry on the Macroscopic Mechanical Properties of a High-Purity  $\text{Y}_2\text{O}_3$ - $\text{Al}_2\text{O}_3$ -Containing Silicon Nitride Ceramic: Role of Oxygen," *J. Am. Ceram. Soc.*, **88** [7] 1900–8 (2005).
- <sup>34</sup>J. J. Kruzic, R. M. Cannon, J. W. Ager III, and R. O. Ritchie, "Fatigue Threshold  $R$ -Curves for Predicting Reliability of Ceramics under Cyclic Loading," *Acta Mater.*, **53** [9] 2595–605 (2005).
- <sup>35</sup>D. Munz, "What can we Learn from  $R$ -Curve Measurements," *J. Am. Ceram. Soc.*, **90** [1] 1–15 (2007).
- <sup>36</sup>C. J. Gilbert, D. R. Bloyer, M. W. Barsoum, T. El-Raghy, A. P. Tomsia, and R. O. Ritchie, "Fatigue-Crack Growth and Fracture Properties of Coarse and Fine-Grained  $\text{Ti}_3\text{SiC}_2$ ," *Scripta Mater.*, **42** [8] 761–7 (2000).
- <sup>37</sup>C. J. Gilbert, J. J. Cao, L. C. De Jonghe, and R. O. Ritchie, "Crack-Growth Resistance-Curve Behavior in Silicon Carbide: Small Versus Long Cracks," *J. Am. Ceram. Soc.*, **80** [9] 2253–61 (1997).
- <sup>38</sup>J. F. Tsai, U. Chon, N. Ramachandran, and D. K. Shetty, "Transformation Plasticity and Toughening in  $\text{CeO}_2$ -Partially-Stabilized Zirconia-Alumina (Ce-TZP/ $\text{Al}_2\text{O}_3$ ) Composites Doped with  $\text{MnO}$ ," *J. Am. Ceram. Soc.*, **75** [5] 1229–38 (1992).
- <sup>39</sup>C. S. Yu and D. K. Shetty, "Transformation Yielding, Plasticity and Crack-Growth-Resistance ( $R$ -Curve) Behavior of  $\text{CeO}_2$ -TZP," *J. Mater. Sci.*, **25** [4] 2025–35 (1990).
- <sup>40</sup>R. Yuan, J. J. Kruzic, X. F. Zhang, L. C. De Jonghe, and R. O. Ritchie, "Ambient to High-Temperature Fracture Toughness and Cyclic Fatigue Behavior in Al-Containing Silicon Carbide Ceramics," *Acta Mater.*, **51** [20] 6477–91 (2003).
- <sup>41</sup>J. J. Kruzic, R. M. Cannon, and R. O. Ritchie, "Crack Size Effects on Cyclic and Monotonic Crack Growth in Polycrystalline Alumina: Quantification of the Role of Grain Bridging," *J. Am. Ceram. Soc.*, **87** [1] 93–103 (2004).
- <sup>42</sup>R. F. Cook, E. G. Liniger, R. W. Steinbrech, and F. Deuerler, "Sigmoidal Indentation-Strength Characteristics of Polycrystalline Alumina," *J. Am. Ceram. Soc.*, **77** [2] 303–14 (1994).
- <sup>43</sup>D. B. Marshall and M. V. Swain, "Crack Resistance Curves in Magnesia-Partially-Stabilized Zirconia," *J. Am. Ceram. Soc.*, **71** [6] 399–407 (1988).
- <sup>44</sup>R. W. Steinbrech and O. Schmenkel, "Crack-Resistance Curves of Surface Cracks in Alumina," *J. Am. Ceram. Soc.*, **71** [5] C271–3 (1988).
- <sup>45</sup>T. Fett and D. Munz, "Influence of Narrow Starter Notches on the Initial Crack Growth Resistance Curve of Ceramics," *Archiv Appl. Mech.*, **76** [11–12] 667–79 (2006).
- <sup>46</sup>N. E. Dowling, "Notched Member Fatigue Life Predictions Combining Crack Initiation and Propagation," *Fatigue Eng. Mater. Struct.*, **2**, 129–38 (1979).
- <sup>47</sup>J. W. Foulk III, R. M. Cannon, G. C. Johnson, P. A. Klein, and R. O. Ritchie, "A Micromechanical Basis for Partitioning the Evolution of Grain Bridging in Brittle Materials," *J. Mech. Phys. Sol.*, **55** [4] 719–43 (2007).
- <sup>48</sup>T. Fett and D. Munz, "Evaluation of  $R$ -Curve Effects in Ceramics," *J. Mater. Sci.*, **28** [3] 742–52 (1993).
- <sup>49</sup>R. W. Steinbrech, A. Reichl, and W. Schaarwächter, "R-Curve Behavior of Long Cracks in Alumina," *J. Am. Ceram. Soc.*, **73** [7] 2009–15 (1990).
- <sup>50</sup>J. C. Hay and K. W. White, "Grain-Boundary Phases and Wake Zone Characterization in Monolithic Alumina," *J. Am. Ceram. Soc.*, **78** [4] 1025–32 (1995).
- <sup>51</sup>K. W. White and J. C. Hay, "Effect of Thermoelastic Anisotropy on the  $R$ -Curve Behavior of Monolithic Alumina," *J. Am. Ceram. Soc.*, **77** [9] 2283–8 (1994).
- <sup>52</sup>A. B. K. Njiwa, T. Fett, J. Rödel, and G. D. Quinn, "Crack-Tip Toughness Measurements on a Sintered Reaction-Bonded  $\text{Si}_3\text{N}_4$ ," *J. Am. Ceram. Soc.*, **87** [1] 1502–8 (2004).
- <sup>53</sup>A. Bhatnagar, M. J. Hoffmann, and R. H. Dauskardt, "Fracture and Subcritical Crack-Growth Behavior of Y–Si–Al–O–N Glasses and  $\text{Si}_3\text{N}_4$  Ceramics," *J. Am. Ceram. Soc.*, **83** [3] 585–96 (2000).
- <sup>54</sup>G. Pezzotti, N. Muraki, N. Maeda, K. Satou, and T. Nishida, "In Situ Measurement of Bridging Stresses in Toughened Silicon Nitride Using Raman Microprobe Spectroscopy," *J. Am. Ceram. Soc.*, **82** [5] 1249–56 (1999).
- <sup>55</sup>M.-Y. He and J. W. Hutchinson, "Crack Deflection at an Interface Between Dissimilar Elastic Materials," *Inter. J. Solids Struct.*, **25** [9] 1053–67 (1989).



<sup>56</sup>D. K. Tran, A. S. Kobayashi, and K. W. White, "Crack Growth in Alumina at High Temperature," *Eng. Fract. Mech.*, **68** [2] 149–61 (2001).

<sup>57</sup>G. Pezzotti, O. Sbaizero, V. Sergo, N. Muraki, K. Maruyama, and T. Nishida, "In Situ Measurements of Frictional Bridging Stresses in Alumina Using Fluorescence Spectroscopy," *J. Am. Ceram. Soc.*, **81** [1] 187–92 (1998).

<sup>58</sup>G. Pezzotti, H. Ichimaru, L. P. Ferroni, K. Hirao, and O. Sbaizero, "Raman Microprobe Evaluation of Bridging Stresses in Highly Anisotropic Silicon Nitride," *J. Am. Ceram. Soc.*, **84** [8] 1785–90 (2001).

<sup>59</sup>J. Rödel, "Crack Closure Forces in Ceramics: Characterization and Formation," *J. Eur. Ceram. Soc.*, **9** [4] 323–34 (1992).

<sup>60</sup>C. J. Gilbert, R. N. Petrany, R. O. Ritchie, R. H. Dauskardt, and R. W. Steinbrech, "Cyclic Fatigue in Monolithic Alumina: Mechanisms for Crack Advance Promoted by Frictional Wear of Grain Bridges," *J. Mater. Sci.*, **30** [3] 643–54 (1995).

<sup>61</sup>G. Pezzotti, I. Tanaka, and T. Nishida, "Intrinsic Fracture Energy of Polycrystalline Silicon Nitride," *Phil. Mag. Lett.*, **67**, 95–100 (1993). □